

## AEROELASTIC TAILORING FOR STATIC AND DYNAMIC LOADS WITH BLENDING CONSTRAINTS

Marco Tito Bordogna<sup>1,2</sup>, Paul Lancelot<sup>2</sup>, Dimitri Bettebghor<sup>1</sup> and Roeland De Breuker<sup>2</sup>

<sup>1</sup>ONERA

The French Aerospace Lab  
F-92322 Châtillon, France  
Marco\_Tito.Bordogna@onera.fr  
Dimitri.Bettebghor@onera.fr

<sup>2</sup>Faculty of Aerospace Engineering

Delft University of Technology  
2629 HS Delft, The Netherlands  
P.M.G.J.Lancelot@tudelft.nl  
R.DeBreuker@tudelft.nl

**Keywords:** Aeroelastic Tailoring, Gust, ESL, Blending, Composite

**Abstract:** In the present paper the authors want to investigate the effect of different load configuration in order to identify the ones driving the optimization. A set of static loads, gust loads and static loads with maneuver load alleviation (MLA) are tested. Gust loads have been included in the optimization via an equivalent static load (ESL). Composite blending is tackled by means of continuous constraints and a two phases approach is proposed to find a blended stacking sequence table. Results show that region of influence can be identified for specific loads and that MLA can be beneficial for structural weight reduction. Finally, the blending constraints prove their effectiveness by significantly reducing the error in retrieving a blended stacking sequence.

## 1 Introduction

Aeroelastic tailoring is a field of research which has received increased attention over the past decades since its very first definition by Shirk et al. [1] in the late 90's . This is thanks to the development of light-weight and highly flexible wings for modern airliners and long endurance aircraft. It has been identified as an efficient way to improve aerodynamic performance while reducing loads and therefore structural weight [2]. Using variable stiffness laminates, the wing structure can be tailored in such way that it will relieve itself from the loads during maneuvers and gusts, while maintaining an optimal aerodynamic shape in cruise. Nonetheless, constraints related to structural strength and stiffness, aeroelastic instability and minimum control effectiveness in flight still apply. All civil aircraft must comply with the certification specifications, and yet be as light as possible. The conventional structural sizing process is mostly driven by fixed loads and by aeroelastic instability constraints [3]. Taking dynamic aeroelastic load cases earlier in the design process could be beneficial in term of performance and could reduce the non-feasibility of the design, Kenway et al. [4] shows that

a wing optimized for fixed loads can fail when subjected to discrete gust. Moreover, these dynamic loads are also influenced by the rigid body motion of the aircraft as shown by Reimer et al. [5] and therefore more difficult to predict.

The use of composite materials to build large structures remains also one of the main challenges of today's aircraft industry. Despite offering improved mechanical performances with higher strength to weight ratio as compared to their conventional aluminium counterparts, composites are more difficult to design because of the increased number of design variables due to the anisotropy of the material and the many manufacturing constraints. Ply angles need to be correctly chosen to determine the optimal stiffness of the laminate in order to minimize or maximize a certain behavior or characteristic of the laminate. Finally, for large composite structure, local section optimization can lead significant thickness and/or stacking sequence variations between adjacent sections. As a consequence, not considering ply continuity (i.e. blending) early in the design phase will reduce structural integrity at sections intersection or could results in hardly manufacturable solutions [6, 7].

Two reference works on static aeroelastic tailoring with local panel optimization are the ones from B. Liu [8] and J. Dillinger [6]. Even though the two works focus on the same topic, they do not use the same problem decomposition approach and they considered blending differently. Liu used a Quasi separable Subsystem Decomposition (QSD) leading to a sequential optimization where the author introduced two blending constraints, one at each step. J. Dillinger used an AIO (*All-in-one*) approach, where a gradient-based (continuous) optimization of homogenized stiffness parameters (e.g. lamination parameters) is performed to obtain the optimum solution. Later a genetic algorithm (discrete optimization) is used to retrieve feasible stacking sequences while enforcing blending.

Several authors have used bi-step strategies, however, due to the difficulties in enforcing discrete blending constraints in the gradient-based optimization, different sets of constraints are used in the two subsequent optimization steps resulting in significant discrepancies between the two solutions. This does no guarantee to find an equivalent of the optimal continuous design in the discrete domain. Recently, Macquart et al. [9] proposed employing lamination parameters combined with a set of blending constraints to be used in the continuous optimization in order to achieve more realistic and manufacturable continuous designs. In [9] the continuous blending constraints have been applied to the benchmark case of the 18 panel horseshoe to prove the effectiveness of the blending method. In a continuing effort, the authors [10] have also demonstrated that the application of blending constraints during aeroelastic optimizations with strain and buckling constraints results in more realistic continuous designs.

In the first part of the paper the authors focus on the identification of the critical loads in aeroelastic tailoring. Static load cases are employed together with gust responses to identify which load configuration is more critical. The effect of performing maneuver load alleviation (MLA) during 2.5g and -1g over the identification of the critical load is assessed. In the second part, an approach to ensure the satisfaction of blending requirements is presented and the effect of the blending over the critical loads is evaluated.

The paper is divided as following. In Sec. 2 the concept of blending is introduced together with the composite parametrization chosen. Then, in Sec. 3 the optimization strategies used in the paper are explained together with the concept of equivalent static load (ESL). The test case used in this work is introduced in Sec. 4 and finally the results are presented and commented in Sec. 5.

## 2 Blending

The use of composite materials to build large structures remains one of the main challenges of today's aircraft industry. Despite offering improved mechanical performances with higher strength to weight ratio as compared to their conventional aluminium counterparts, they are more difficult to design because of the increased number of design variables due to the anisotropy of the material and the many manufacturing constraints. Moreover, in order to obtain better performing structures, large components are usually divided in sections each of them locally optimized with respect to thickness and composite anisotropy. As consequence the optimization process could result in optimal solution that lack of structural integrity because of significant thickness and/or stacking sequence variations between adjacent sections. Therefore, constraints over ply continuity (i.e. blending) should be taken into account early in the design phase in order to obtain ready-to-manufacture solutions [6,7].

Several definitions of blending have been proposed (Figure 1). Inner and outer blending have been introduced by Adams et al. [11], in these definitions only the innermost and the outermost plies can be dropped. Two alternative definitions, the generalized and relaxed generalized blending, have been formulated by Van Campen et al. [12]. Generalized blending requires all plies of the thinnest section to be continuous in the whole structure; relaxed generalized blending demands that no discontinuous plies should be in direct physical contact with each other. Throughout this paper, blending is always associated to the generalized blending definition of Van Campen et al. [12] for sake of clarity.

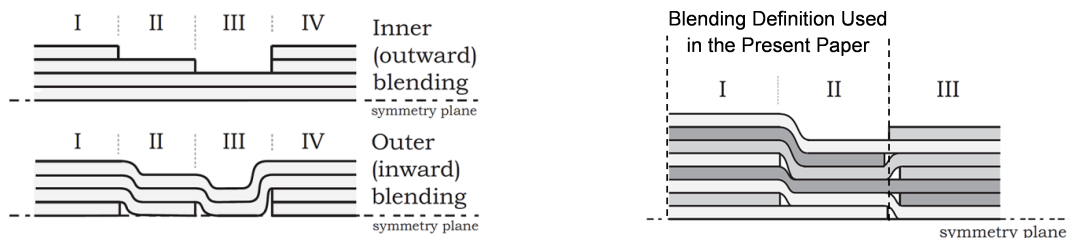


Figure 1: Outward and inward blending on the left, and generalized (I and II) and relaxed generalized (II and III) blending on the right. Original figures from [12].

In this work, blending among adjacent sections is enforced by means of the continuous blending constraints introduced by Macquart et al. [9] in the lamination parameter space. Lamination parameters (LPs) have been first introduced by Tsai et al. [13] and are used to describe the stiffness matrix of composite laminates in a continuous space. For stacking

sequence with discrete plies of constant thickness ( $t_{ply}$ ) and ply angle ( $\theta_i$ ), lamination parameters are defined in Eqs. 1. In this paper only symmetric stacking sequence with even number of ply and same thickness are considered, therefore only lamination parameters for membrane ( $A$ ) and bending ( $D$ ) stiffness matrices are taken into account.

$$\begin{aligned} (V_1^A, V_2^A, V_3^A, V_4^A) &= \frac{1}{N} \sum_{i=1}^N (\cos 2\theta, \sin 2\theta, \cos 4\theta, \sin 4\theta) dz \\ (V_1^D, V_2^D, V_3^D, V_4^D) &= \frac{4}{N^3} \sum_{i=1}^N z_i^2 (\cos 2\theta, \sin 2\theta, \cos 4\theta, \sin 4\theta) dz \end{aligned} \quad (1)$$

where  $z_i = -N/2 + i$

Lamination parameters (LPs) have the advantages of describing the stiffness matrix in a continuous and they define a convex space [14] suitable for gradient-based optimizers. Moreover, any generic stacking sequence can be reproduced with twelve continuous variable plus laminate thickness. On the other hand the use of LPs requires an additional optimization step (usually performed by evolutionary algorithms) that retrieves a discrete stacking sequence from the continuous optimum. Therefore a two phase optimization strategy is required (see Sec. 3).

The key concept for the derivation of the continuous blending constraints is to evaluate the change in lamination parameters ( $\Delta V$ ) due to ply drops. A comprehensive derivation of all the blending constraints can be found in [9]. Here for safe of completeness, the derivation of the blending constraints for a single in-plane lamination parameter (Eq. (6)) is presented.

Lets denote  $V_{1(N)}^A$  and  $V_{1(N-X)}^A$  the value of the first in-plane lamination parameter when the laminate has respectively  $N$  and  $N - X$  plies. The change in lamination parameter due to a  $X$  ply drops is denoted as  $\Delta V_{1(N) \rightarrow (N-X)}^A$  and it is presented in Eq. (4).

$$V_{1(N)}^A = \frac{1}{N} \sum_{i=1}^N \cos(2\theta_i) \quad (2)$$

$$V_{1(N-X)}^A = \frac{1}{N-X} \sum_{i=X+1}^N \cos(2\theta_i) \quad (3)$$

$$\Delta V_{1(N) \rightarrow (N-X)}^A = V_{1(N)}^A - V_{1(N-X)}^A = \underbrace{\frac{1}{N} \sum_{j=1}^X \cos(2\theta_j)}_{\text{Term containing the dropped plies}} + \underbrace{\left( \frac{1}{N} - \frac{1}{N-X} \right) \sum_{i=1}^{N-X} \cos(2\theta_i)}_{\text{Term containing the plies present in both sections}} \quad (4)$$

where  $X$  is the number of dropped plies,  $N$  is the total number of plies,  $\theta_j$  represent the orientation of the dropped plies and  $\theta_i$  the orientation of the plies left in the stacking sequence. The maximum and minimum value of Eq. (4) occurs respectively for  $[\theta_j, \theta_i] = [0^\circ, 90^\circ]$  and for  $[\theta_j, \theta_i] = [90^\circ, 0^\circ]$  at which  $\Delta V_{1(N) \rightarrow (N-X)}^A$  is:

$$\max_{(\theta_j, \theta_i)} \|\Delta V_{1(N) \rightarrow (N-X)}^A\| = 2 \frac{X}{N} \quad (5)$$

This implies that no blendable solution can be found if, in two adjacent sections, the change in  $V_1^A$  is greater than  $2(X/N)$ . By applying the same approach to the remaining in-plane

lamination parameters, it can be shown that this limit holds. Thus, it is possible to define a blending constraint for single in-plane lamination parameter change as:

$$\|\Delta V_{k(N) \rightarrow (N-X)}^A\| \leq 2 \frac{X}{N}, \quad \text{for } k = 1, 2, 3, 4 \quad (6)$$

For sake of brevity, the extension of the blending constraints to the higher dimension (i.e. taking into account more LPs) is not covered and the interested reader is invited to check the work of Macquart et al. [9]. However, in order to provide the reader with a visual representation of the constraints, an example of the effect of a 2D blending constraints considering  $V_1^A$  and  $V_2^A$  is hereby provided. Lets take into account the situation presented in Figure 2, where a multi-section laminate is subjected to  $X$  ply drops from a section with  $N$  plies to another with  $N - X$  plies. Lets now reproduce this situation in the lamination parameters space for  $V_1^A$  and  $V_2^A$  (Figure 3). In this example the starting laminate section has  $N$  equal to 20 plies and it is used to generate all possible  $N - X$  plies blended sections by removing  $X$  equal to 2 and 4 plies. Blending constraints for the two different ply drops are shown to be capable of including all possible  $N - X$  plies blended sections. A shrinking factor  $\alpha$  is added to the constraints to reduce the hypersphere created by the blending equations and therefore tighten the constraints

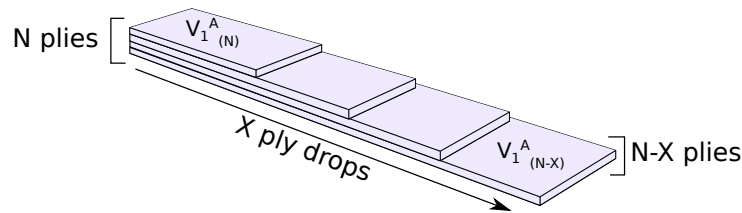


Figure 2: Multi-section laminate and ply-drops illustration

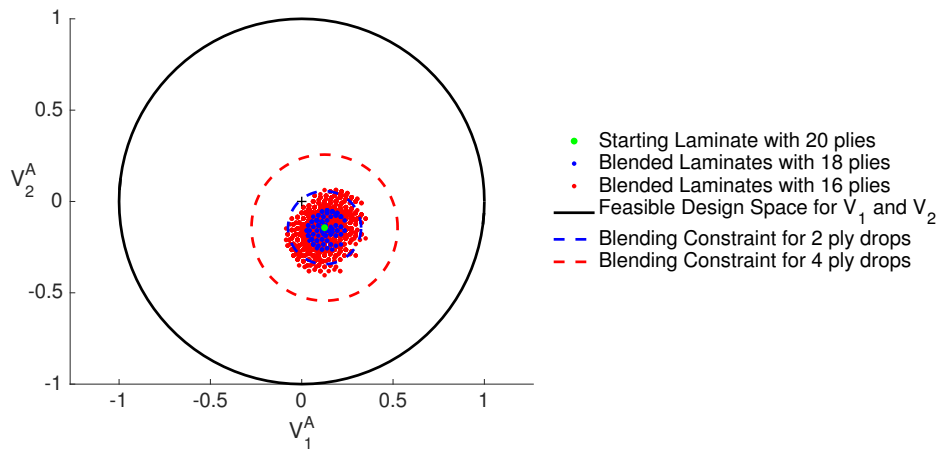


Figure 3: Example of a 20 plies laminate and all its possible blended laminates with 2 and 4 ply drops.

### 3 Optimization strategy

In this section the optimization strategy is explained. As already mentioned in Sec. 2, the use of lamination parameters require a two-phases approach where a continuous gradient-based

optimization is followed by an inverse optimization problem where, from the optimum LPs, the corresponding stacking sequence is retrieved. The full two-phases optimization is introduced in Sec. 3.2 while in Sec. 3.1 the concept of the equivalent static load (ESL), fundamental to consider the gust case in the optimization, is presented and its implementation explained.

### 3.1 Equivalent Static Load (ESL)

To perform this optimization, a gradient-based approach is preferred as the number of design variables is relatively large ( $\approx 400$ ). One issue when accounting for gust loads remains that these loads are highly dependent on the design itself. They are constantly changing during the optimization, as the design evolves with it. However the computation of required sensitivity over a transient response is not an easy task and can require a lot of function evaluations [15]. Therefore, transient responses are costly to implement into current design optimization process. The equivalent static loads (ESL) method formalized by Kang et al. [16] is used to bypass this issue and provides optimized results for static and dynamics load cases.

In the present work ESL is used with little improvement regarding the original idea as described in Figure 4. Nonetheless, it is worth mentioning that examples of improved ESL method exist in the literature. For instance, Bettebghor et al. [17] proposed to estimate the load sensitivities with surrogate modeling. This work was applied to engine pylon sizing in the event of a "fan blade off", a highly dynamic load case. ESL was extended to different scenarios, most of them summarized by Park [18]. These include non-linear geometries, multi body dynamics, and crash and topology optimization for the automotive industry.

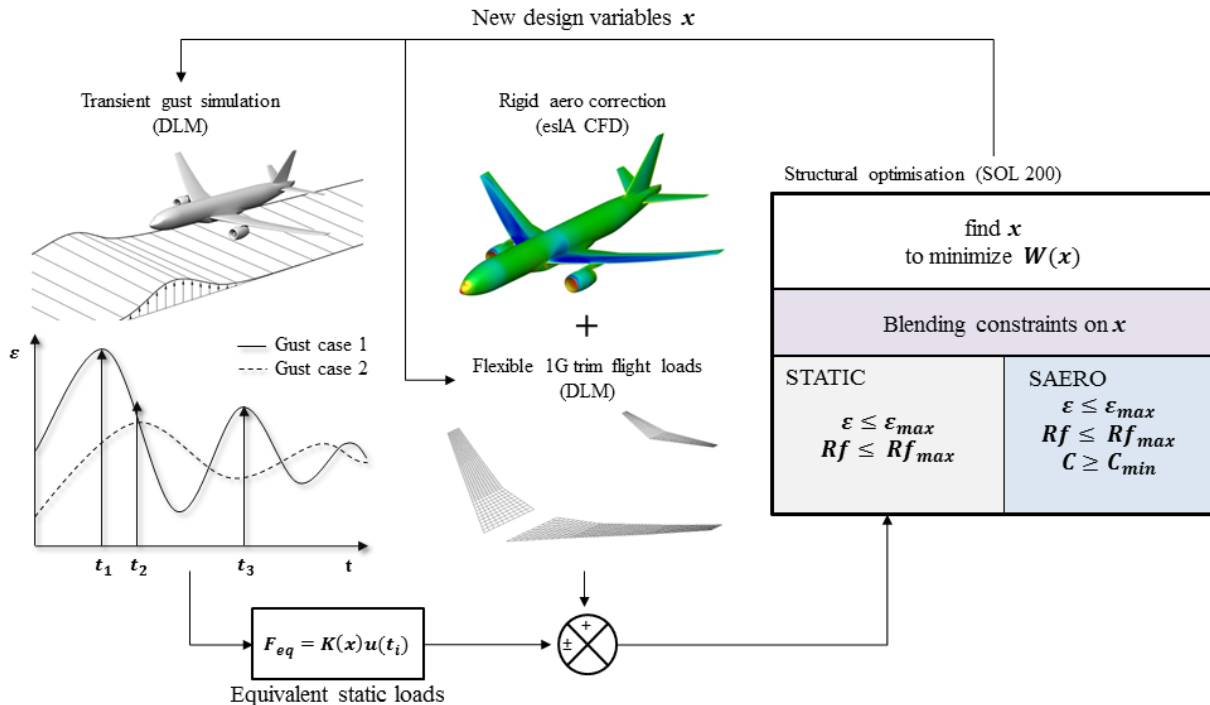


Figure 4: Overview of the equivalent static load process. ELS is incorporated in step 1 and 2 of the optimization process (Sec.3.2).

ESL relies on a weak coupling between the transient simulations and the optimizer. Therefore, it requires several iterations where loads are updated along the new design before a converged solution emerges. The lack of sensitivities between the design variables and the transient responses constitutes one of the main drawback of this method. Therefore, design changes between two consecutive ESL loop need to be small enough to ease constraints satisfactions. Still, this method offers an easy implementation regardless of the different tools used in the loop and can take advantage of already existing gradient based optimization and aeroelastic analysis code. The governing equation that needs to be solved for a gust analysis is the following:

$$M(x)\ddot{u}(t) + K(x)u(t) = f_{\text{gust}}(v_{\infty}, v_{\text{gust}}(t), \ddot{u}(t), u(t)) \quad (7)$$

where  $u$  is the nodal displacement vector,  $M$  and  $K$  respectively the mass and linear stiffness matrices which are dependent upon the design variables  $x$  and  $f_{\text{gust}}$  the aerodynamic forces due to a gust. Finally,  $v_{\text{gust}}$  is the vertical speed component of a transient gust and  $v_{\infty}$  the flow speed in the far field. No structural damping is required as the damping forces are provided by the aerodynamic part. Once the displacements computed from the Eq. 7, a set of equivalent static loads  $f_{\text{eq}}$  can be retrieved from the time steps identified in the elements strain history as the most critical:

$$f_{\text{eq}} = K(x)u(t_i) \quad (8)$$

In the case of a free flying aircraft simulation, the structural displacements are obtained by removing the rigid body translations and rotations from the displacement vector of each grid points. The loads are computed at each iteration with the transient aeroelastic module of MSC.Nastran, designated as the Solution 146. This solution relies on the Doublet Lattice Method (DLM) to solve the gust analysis problem. Although Eq. 7 is given as time dependent, MSC.Nastran solves everything in the frequency domain before converting the output results (displacement, strains etc.) in the time domain. This method is limited to linear aerodynamic and structural computation only. Once the set of ESL generated, they are sent to the optimizer module of MSC.Nastran (SOL200) to be treated as a static structural optimization problem. SOL200 can also compute steady aeroelastic loads for which the optimizer has access to the sensitivities and efficiently perform gradient based optimization. In this example the constraints are applied on strength ( $\epsilon$ ), on the buckling reserve factor ( $RF$ ) and on the minimum static aileron efficiency ( $C_{min}$ ). These are described more in depth Sec. 4.2.

### 3.2 Continuous and Discrete Optimization phases

The full two-phases optimization process is presented in Figure 5. The first phase (Sec. 3.2.1) present the continuous optimization where the optimal LPs are obtained through a gradient-based process performed via MSC.Nastran SOL 200. Once the optimal LPs have been found, the corresponding stacking sequence is identified by mean of an inverse optimization problem via genetic algorithm (Sec. 3.2.2).

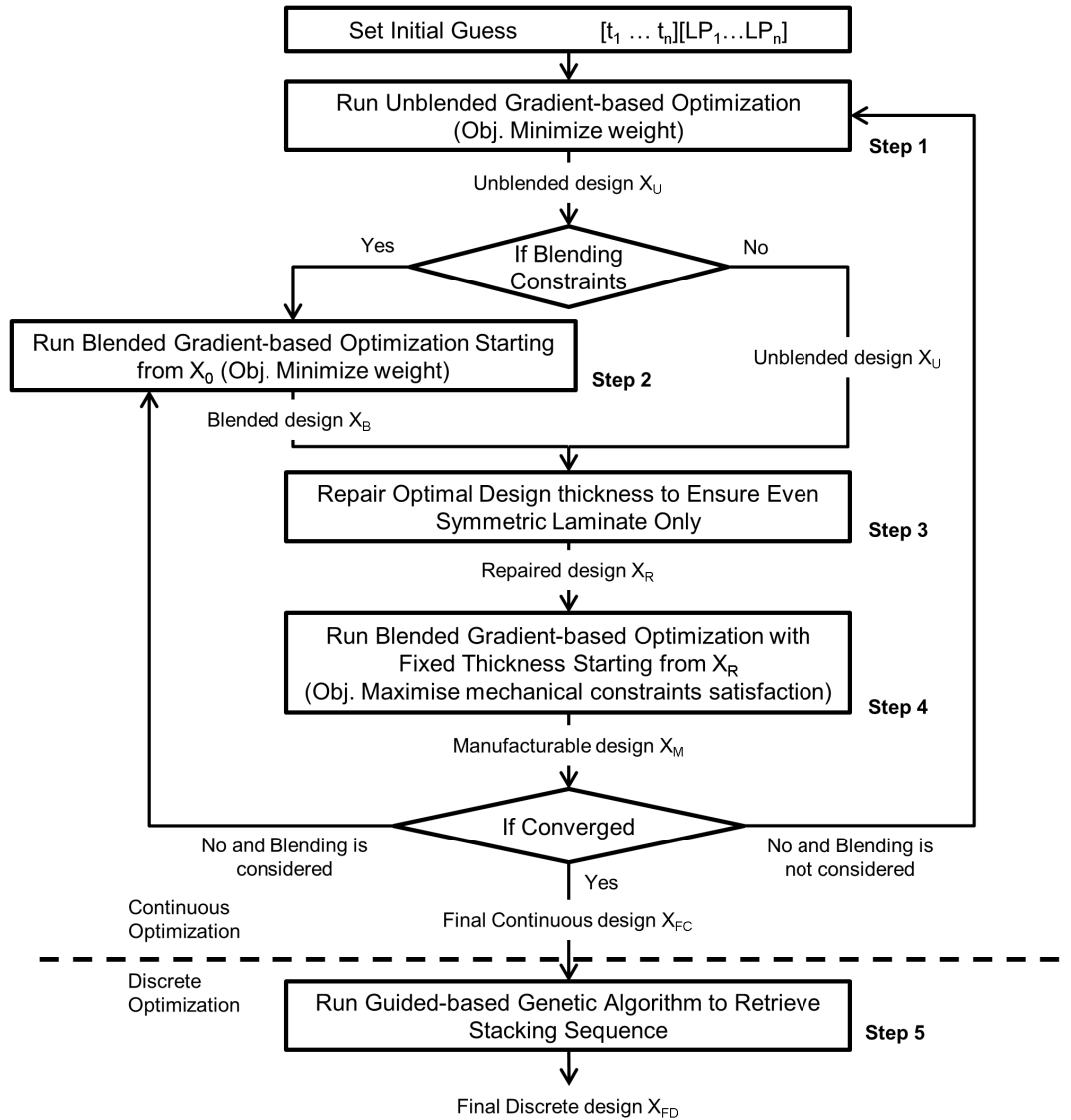


Figure 5: Proposed optimization strategy including blending constraints.

### 3.2.1 Continuous optimization

The blending constraints limit the change of lamination parameters between each section as function of their change in thickness. Applying those constraints while simultaneously optimizing thickness and lamination parameters leads to a non-convex optimization problem. Therefore, a 4-step strategy is employed in phase one or the optimization strategy (Figure 5).

For the case where blending constraints are enforced. The first step of this algorithm is the conventional convex optimization of the structure thicknesses and lamination parameters without blending constraints. This step provides a feasible starting point before the introduction of the blending constraints. The unblended design ( $X_U$ ) is used as starting point for step 2, where blending constraints are considered. In step 3, a repair function rounds up the thicknesses of blended design ( $X_B$ ) to an even number of plies. After the repaired



design ( $X_R$ ), lamination parameters are optimized one last time in step 4 while thicknesses are fixed. During this step, the feasibility of the structure is maximized, meaning that the objective function during this step is to maximize the reserve factors of all the mechanical constraints. Rounding of thicknesses and maximizing of reserve factors modify the stiffness of the structure, leading to internal load redistribution. Therefore, step 2-4 are repeated until convergence to a final continuous design ( $X_{FC}$ ). After the final continuous design is obtained, a stacking sequence retrieval GA is employed to retrieve a blended final discrete design ( $X_{FD}$ ). In case blending is not required, step 2 is avoided and steps 1,3-4 are repeated until convergence. The overall strategy is presented in Figure 5.

The optimizer and FEM solver used in this optimization is MSC.Nastran SOL 200, whereas the proposed strategy is implemented and run externally via Matlab script. The doublet lattice method (DLM) used to compute aeroelastic loads inside the static aeroelastic solver SOL144 have been corrected with rigid CFD computation to consider for wing profile camber and twist law (see Sec. 4.4).

### 3.2.2 Discrete optimization - Stacking sequence retrieval

The OptiBLESS [19] open source stacking sequence optimization toolbox is used to retrieve manufacturable laminates <sup>1</sup>. OptiBLESS uses a guide-based GA in order to retrieve blended stacking sequences matching the optimized lamination parameters achieved by the gradient-based optimizer (i.e. MSC.Nastran). According to the guide-based methodology [11], the thickest laminate is defined as the guide-laminate. Other laminates from the same structure are obtained by dropping plies from the guide-laminate therefore ensuring the final design is blended.

The outcome of the continuous optimization step is used as starting point for the discrete optimization. After the continuous optimization each wing section is optimized in terms of laminate thickness and lamination parameters. The thickest laminate within each substructure (i.e. skins and spars) is identified and set as the guide. Next, the ply angles describing the guide laminate stacking sequence and ply drops are used as design variables in OptiBLESS. Doing so ensure some level of structural continuity between each of the substructure laminates. That is, the plies of thinnest top skin laminate are ensured to span the entire top skin structure due to the guide-based coding implemented in OptiBLESS.

The genotype used in OptiBLESS to describe composite structures is given as:

$$Genotype = \left[ \underbrace{[\theta_1 \theta_2 \dots \theta_n]}_{\text{Ply angles}} \underbrace{[\Xi_1 \Xi_2 \dots \Xi_D]}_{\text{Drop off}} \right] \quad (9)$$

The guide laminate is fully defined by the  $\theta$ 's. Other laminates are obtained by dropping plies from the guide stacking sequence. Since the number of plies associated with each section

<sup>1</sup><https://github.com/TMacquart/OptiBLESS>

of structure is known from the continuous optimization, the ply drop off design variables denote which ply of guide stacking sequence must be dropped.

The objective function used during the discrete optimization represents the lamination parameter matching quality between the continuous and discrete design. In other words, OptiBLESS is set to retrieve blended stacking sequences with lamination parameters matching the lamination parameters obtained at the end of the continuous optimization. This objective function is simply expressed as the root mean square error (RMSE) between the continuous and discrete lamination parameters as shown in Eqs. (10 and 11).

$$Fitness(\boldsymbol{\theta}, \Xi) = \frac{1}{N_{lam}} \sum_{s=1}^{N_{lam}} RMSE_s(\boldsymbol{\theta}, \Xi) \quad (10)$$

$$RMSE_s(\boldsymbol{\theta}, \Xi) = \sqrt{\frac{1}{8} \sum_{i=1}^8 w_i (\widetilde{\mathbf{LP}}_{i,s} - \mathbf{LP}_{i,s}(\boldsymbol{\theta}, \Xi))^2} \quad (11)$$

where  $N_{lam}$  is the total number of laminate sections in a structural component (i.e. upper wing skin),  $\widetilde{\mathbf{LP}}_{i,s}$  is the vector of input parameters for section  $s$ ,  $w_i$  is a weighting factor and  $\mathbf{LP}_{i,s}$  is the vector of lamination parameters obtained by the GA. Stacking sequences are converted into lamination parameters in order to evaluate the fitness using the following notation:

$$\mathbf{LP} = [V_1^A \ V_2^A \ V_3^A \ V_4^A, \ V_1^D \ V_2^D \ V_3^D \ V_4^D] \quad (12)$$

According to the fitness function given in Eq. (10), the best retrieved stacking sequence would be a manufacturable stacking sequence exactly matching the optimized lamination parameters obtained by MSC.Nastran.

## 4 Model Description

### 4.1 Structural Model Description

The shell FE shell model is characterized by upper and lower skins, front and rear spars, 32 ribs, 13 stringers and represents a realistic aircraft regional aircraft wing. The structure is divided in sections each of them locally optimized by means its thickness and composite material anisotropy. In total there are 44 section, 14 for each skins and 8 for each spars Figure 6). Ribs and stiffeners do not take part in the optimization and are made of quasi-isotropic composite. Wing dimensions are presented in Table 1.

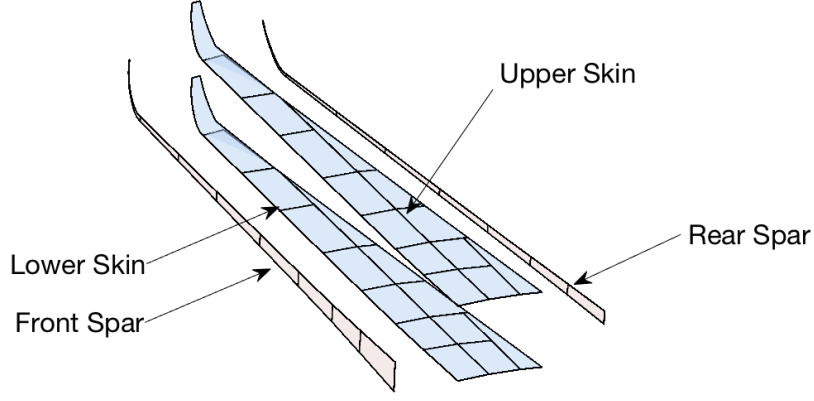


Figure 6: Wing used in the optimization divided in different section for local optimization.

Wing geometric characteristics	
Half Wingspan	16.7 m
Wing Area	111 m <sup>2</sup>
Wing Dihedral	3.5°
Leading edge Sweep Angle	18°
MTOW	60,000 kg
Design cruise Mach	0.75

Table 1: Wing features.

## 4.2 Constraints

Two sets of structural constraints are active on the model. One set of constraints is represented by the material compatibility equations [20], these constraints ensure that each set of in-plane and out-of-plane lamination parameters leads to a realistic A and D stiffness matrix. The second set of constraints ensure that the model satisfies mechanical requirements such as strength and local buckling

The strength constraint used have been derive by IJsselmuiden et al. [21] and represent an analytical expressions for a conservative failure envelope based on the Tsai-Wu failure criterion in strain space. Local buckling is constrained via the closed formula Eq. (13) in all regions delimited by two ribs and two stiffeners and is enforced only in the wing skins.

$$\lambda_B = \pi^2 \frac{D_{11}(m/a)^4 + 2(D_{12} + 2D_{33})(m/a)^2(n/b)^2 + D_{22}(n/b)^4}{(m/a)^2 N_X + (n/b)^2 N_Y} \quad (13)$$

where buckling occurs for  $\lambda_B < 1$ ,  $N_X$  and  $N_Y$  are the stresses in the longitudinal and transverse directions,  $a$  and  $b$  are the corresponding region dimensions and  $m$  and  $n$  are the corresponding number of half waves. A safety margin of 50% is applied to both strength and local buckling criteria.

A constrain on minimum aileron effectiveness is also imposed. It is formulated as follow:

$$C_{\min} = \frac{M_{\text{elastic}}}{M_{\text{rigid}}} \quad (14)$$

where  $M_{\text{rigid}}$  is the root bending moment created by deflecting the aileron on the rigid model, and  $M_{\text{elastic}}$  on the flexible model.  $C_{\text{min}}$  is constrained such as its value does not go below  $10^{-4}$  at 1.2 times the speed reaching the maximum dynamic pressure.

### 4.3 Loadcases

Different load cases are used in the optimization process. Table 2 summarized the manoeuvre loads:

N	Name	Mach	Altitude (ft)	Load factor (g)
1	Pull up	0.48	0	2.5
2	Push down	0.48	0	-1
3	Reversal	0.605	0	1

Table 2: List of the steady load cases used in the optimization.

As described in figure 4, the incremental gust loads are added to 1g flight loads, also computed at Mach 0.48. The different gust cases are summerize Table 3:

N	Frequency (Hz)	Gust angle(deg)
1	9.06	5.94
2	7.40	6.15
3	5.73	6.42
4	4.07	6.79
5	2.40	7.42
6	0.74	9.02

Table 3: List of gust cases.

### 4.4 DLM correction

The aeroelastic loads are calculated via the MSC.Nastran static aeroelastic solver the utilize doublet lattice method (DLM). Since the aeroelastic loads coming from the DLM are use perform trim of the wing and calculate its displacement, it is important to correctly represent the spanwise and chordwise load distribution along the wing. This is achieved by using the concept of separation between the rigid and elastic load components, where the rigid part utilize rigid CFD results while the elastic increment is computed via DLM. This method, offer referred to as hybrid static approach [22], allows to consider in the aeroelastic load computation for airfoil camber and wing twist law. This, not only ensures a more realistic lift distribution for structural sizing, but also provide correct wing deflection to the surrogate model so that the flexible load increment effect on on aerodynamic performance will be realistic, improving the fidelity of aircraft performance evaluation.

## 5 Results and Comments

### 5.1 Continuous step

In this section, results from various continuous optimizations are discussed. All optimizations performed in this section have been done using the approach showed in Sec. 4 where each of the loads were included when needed.

First the effect of the inclusion of dynamic loads on the structure is assessed. The weight of the composite wing box optimized with only static loads, as shown in Table 2, is 593.6 kg while the inclusion of gust loads increases it to 636.4 kg. In Figure 7, the importance of each load cases in the sizing process underlined by highlighting the critical load case in each element of buckling section. One can observe that, while gusts have limited effect on buckling, they are more critical for strength and affects more the outer part of the wing close to the trailing edge. As expected, the pull-up maneuver mostly sizes the upper skin in buckling, as well as most of the root for strength. Moreover, the pull-up is also critical in grand part of the lower skin in strength. The push-down on the other hand is the sizing load for the lower skin in buckling, and for the upper skin close to the leading edge in strength. In the present work only one mass configuration is considered together with a limited number of load cases, thus the results could differ if case of extension to a greater spectrum of load cases.

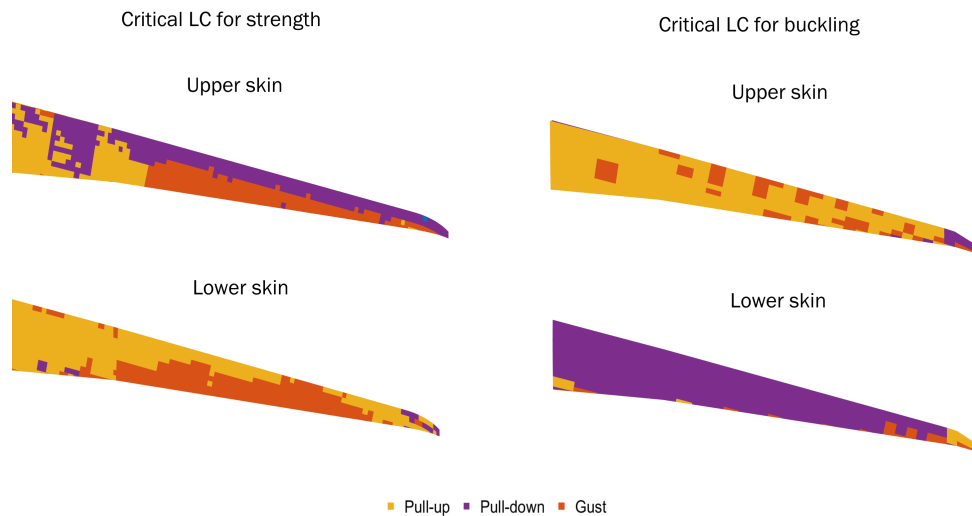


Figure 7: Critical critical load cases with respect to strength and buckling constraints.

The effect of maneuver load alleviation (MLA) on the structural design is also assessed. While aileron deflection can relieve some root bending moment, it can also induce additional torsional loads, due to the aileron location at the rear of the wing. The best way to solve this trade-off is to resize the wing box and re-evaluate the weight for different aileron deflection values. For this study, only the +2.5g and -1g load cases are used. Non-linear aerodynamic model at the aileron, such as flow separation around the hinge, is not implemented. Aileron reversal constraint is accounted for.

The results of the study are plotted in Figure 8. One can observe that in case of a purely continuous optimization (no thickness round-up and no blending constraints) the wing

weight will decrease as the aileron deflection increases. This isn't true anymore if blending constraints are used, inducing a minimum weight for 35° deflection. This could be explained as a result of the wing not being fully tailored for the more complex load path induced by a high aileron deflection. It can be observed that prior to the optimal deflection, the weight penalty induced by the blending constraints is relatively constant. Finally, only the deflection angle for the 2.5g load case is presented here however MLA is also applied during the -1g load case. A similar aileron deflection is applied, but divided by -2.5.

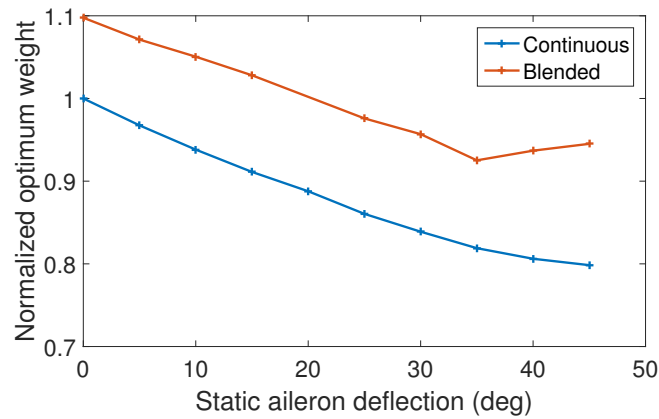


Figure 8: Optimum weight for various aileron deflection angle, with and without blending.

## 5.2 Discrete step

Among the tests performed in Sec. 5.1 the test case with static loads plus gusts have been used here to show the effectiveness of the blending constraints and the optimization strategy proposed in Sec. 3.2. Two different optimizations have been run, one without the blending constraints and one with the constraints and a shrinking factor  $\alpha$  set to 0.5.

The difference in weight of the optimized solutions is shown in Figure 10 and lead to an increase of weight of about 4.65%. This weight increment is coherent with the reduction of the design space due to the inclusion of additional constraints. In Figure 9 the averaged RMSE obtain from 10 different stacking sequence retrieval is shown for the different problems. Results show that, even if not perfect match has been found in neither cases, stacking sequences closely matching the continuous optimum can be obtained thanks to the use of the blending constraints.

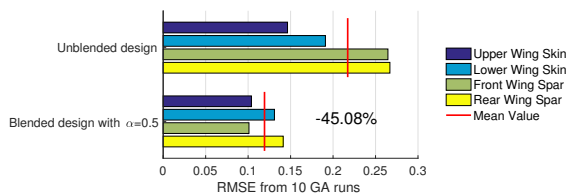


Figure 9: RMSE in stacking sequence retrieval via GA averaged over 10 runs.

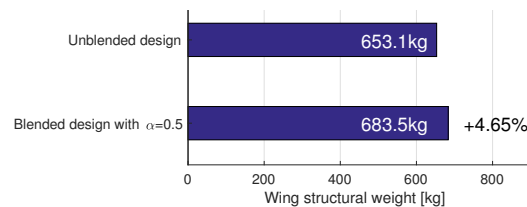


Figure 10: Weight of the optimized wing structure under static and gust loads.

Figures 12 and 12 present the thickness distribution for the two solutions. The solutions obtained with the blending constraints increases thickness uniformly along the full wing.

This change in thickness is reflecting a change in stiffness orientation (see Figures 13 and 14). The stiffness orientation [6] represent the value of the in-plane stiffness component  $A_{11}$  in the panel and therefore allows for a visual representation of the main fiber direction. In the blended solution, thicknesses and stiffness directions in each panes are interconnected by means of the blending constraints. Therefore, the optimized is balancing the stiffness coming from thickness and from anisotropy in order to satisfy the blending requirements.

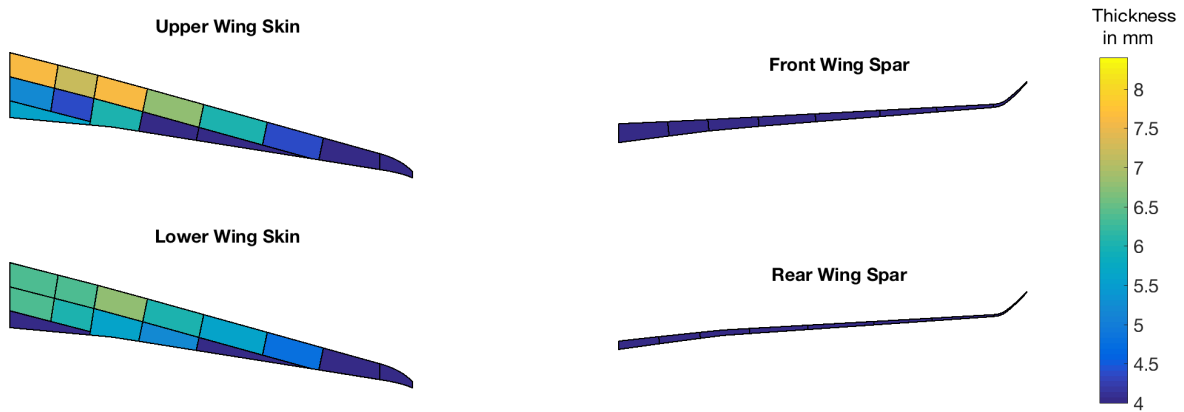


Figure 11: Thickness distribution along the wing for the unblended design.

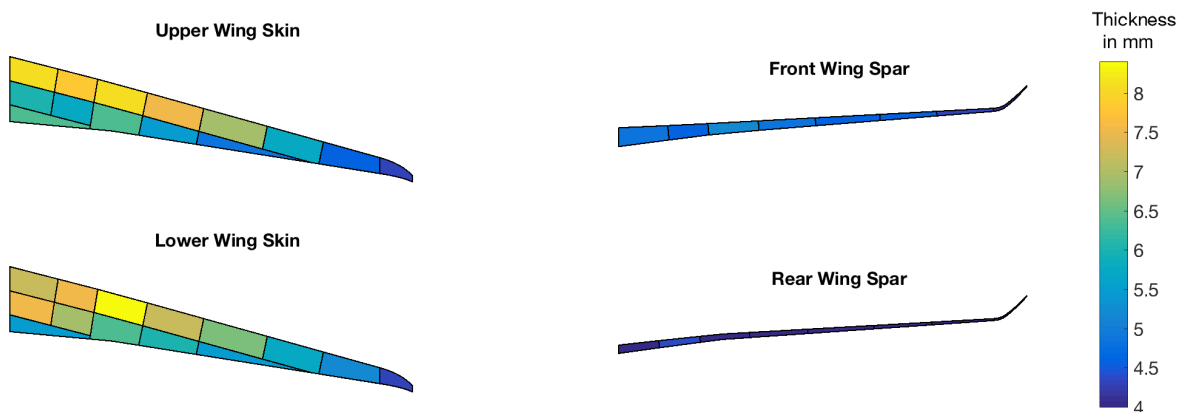


Figure 12: Thickness distribution along the wing for the blended design.

Spanwise and chordwise stiffness variation between the blended and unblended design is shown how the use of blending constraints helps in reducing stiffness local variation and results in a smooth variation between wing root and wing tip. This latter effect is clearly visible by comparing the lower skin and the front spar results shown in Figures 13 and 14.

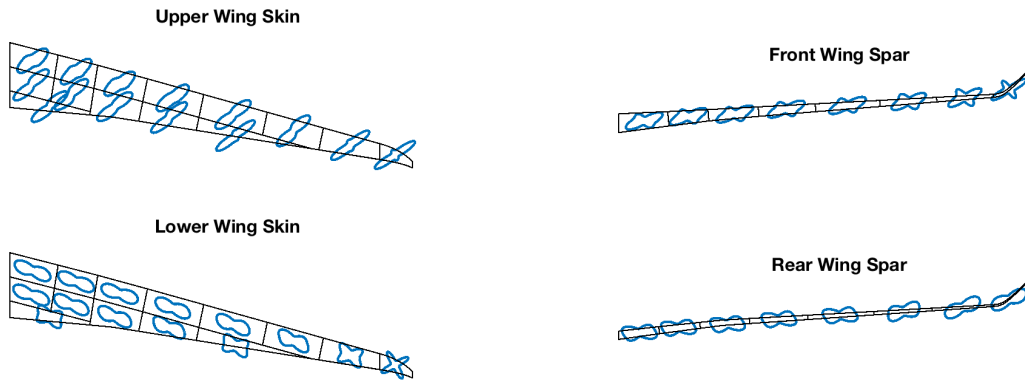


Figure 13: Stiffness distribution along the wing for the unblended design.

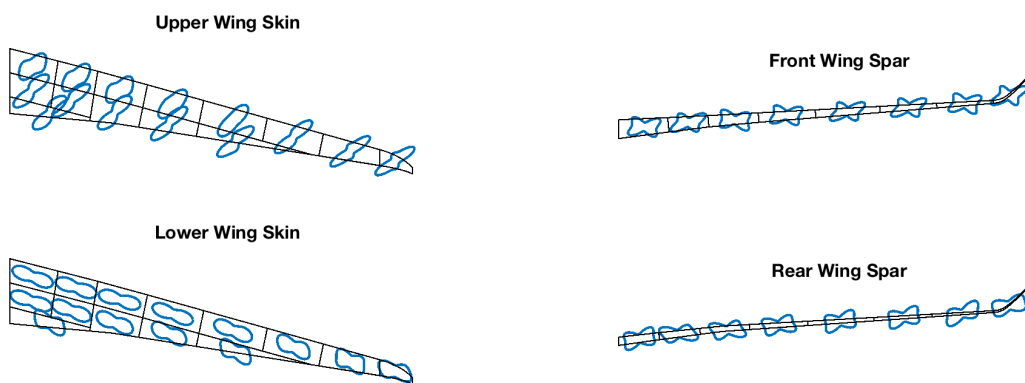


Figure 14: Stiffness distribution along the wing for the blended design.

However, even if blending constraints helped the optimized to find a continuous solution that could be more closely match by a discrete stacking sequence, the RMSE is still non zero (Figure 9). This means that while all constraints have been satisfied during the continuous optimization (see Figure 15), the now retrieved discrete stacking sequences are not guaranteed to fulfill all mechanical constraints. Figures 15 and 16 show the valued of the mechanical constraints (i.e. strength and local buckling) at the end of the continuous optimization step and after the stacking sequence retrieval. Clearly enough not obtaining a 100% match between continuous and discrete designs leads to mechanical constraints violation with or without blending constraints. However, the use of the blending constraints greatly reduce the number for failed constraints and the magnitude of the failure indices (Table 4).



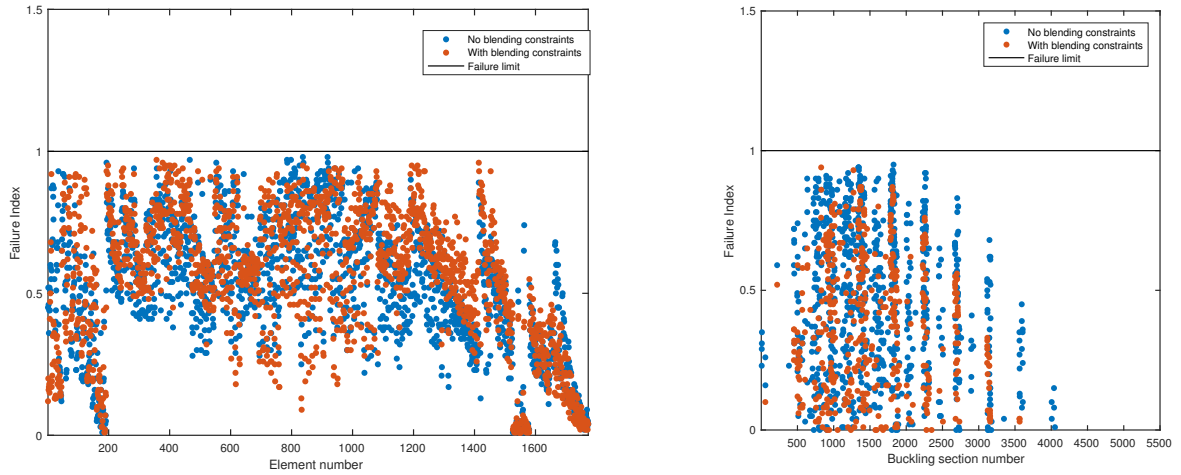


Figure 15: Strength and buckling violated constraints at the end of the continuous optimization.

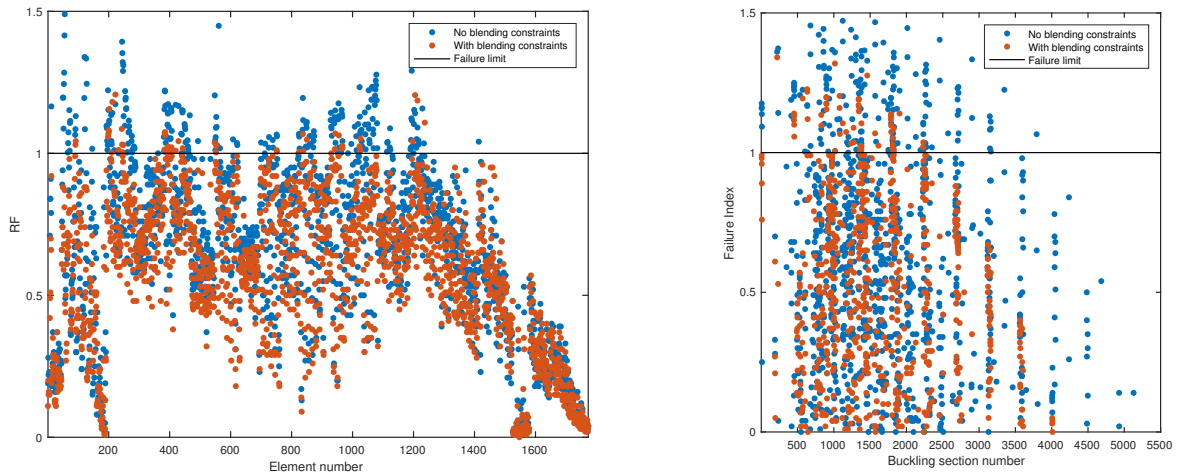


Figure 16: Strength and buckling violated constraints after stacking sequence retrieval.

Mechanical constraint	Failed Elements		Averaged Failure Indices	
	No Blending	With Blending	No Blending	With Blending
Strength	230	52	0.1428	0.0714
Local Bucking	158	60	0.2214	0.1332

Table 4: Improvements in constraints violation after stacking sequence retrieval due to the use of blending constraints.

## 6 Conclusions and further works

The present paper investigates the effect of different load configurations in order to identify region of influence for different loads. The loads considered in the current work are static loads, gust loads and static loads with maneuver load alleviation (MLA). Gust loads have been included in the aeroelastic optimization via an equivalent static load (ESL). The different loads

are applied to a regional aircraft composite wing that is optimized with respect to local panel thickness and composite anisotropy. Composite blending is tackled by means of continuous constraints and a two phases approach is proposed to find a blended stacking sequence table.

Results have shown that region of influence can be identified for specific loads. Moreover, the inclusion of the gust load in the structural optimization resulted in approximately 10% weight increment, thus confirming the importance of considering gust loads during preliminary design. MLA has been applied to the 2.5g and -1g load cases, without gust, showing its potential capabilities in reducing structural weight up to 20%. A smaller weight reduction have been found when blending has been taken into account.

Finally, the composite wing structure under static and gust loads has been optimized with and without the blending constraints. The use of the blending constraints reduced by approximately 45% the RMSE of the generic algorithm used to retrieved a blended stacking sequence. However this came at the price of a heavier design (+4.65%) due to the reduce design space. The reduced RMSE coming from the use of the blending constraints resulted in significant reduction of failed element and failure indices in the retrieved stacking sequence.

Further works will include multiple mass configurations for gust computations as well as different flight conditions, non-linear aerodynamics effect on aileron deflection for MLA and improvements in the stacking sequence retrieval performed via generic algorithm.

## 7 References

- [1] Shirk, M. H., Hertz, T. J., and Weisshaar, T. A. (1986). Aeroelastic tailoring - theory, practice, and promise. *Journal of Aircraft*, 23(1), 6–18. doi:<http://dx.doi.org/10.2514/3.45260>.
- [2] Jutte, C. and Stanford, B. K. (2014). Aeroelastic Tailoring of Transport Aircraft Wings: State-of-the-Art and Potential Enabling Technologies. Tech. rep.
- [3] Grihon, S., Krog, L., and Bassir, D. (2009). Numerical Optimization applied to structure sizing at AIRBUS: A multi-step process. *International Journal for Simulation and Multidisciplinary Design Optimization*, 3(4), 432–442. ISSN 1779-627X, 1779-6288. doi: 10.1051/ijsmdo/2009020.
- [4] Kenway, G., Kennedy, G., and Martins, J. R. R. A. (2014). Aerostructural optimization of the Common Research Model configuration. In *15th AIAA/ISSMO Multidisciplinary Analysis and Optimization Conference*.
- [5] Reimer, L., Ritter, M., Heinrich, R., et al. (2015). CFD-based Gust Load Analysis for a Free-flying Flexible Passenger Aircraft in Comparison to a DLM-based Approach. In *22nd AIAA Computational Fluid Dynamics Conference*.
- [6] Dillinger, J. K. S. (2014). *Static Aeroelastic Optimization of Composite Wing with Variable Stiffness Laminates*. Ph.D. thesis, Delft University of Technology.

- [7] Ijsselmuiden, S. T., Abdalla, M. M., Seresta, O., et al. (2009). Multi-step blended stacking sequence design of panel assemblies with buckling constraints. *Composites Part B: Engineering*, 40(4), 329 – 336. ISSN 1359-8368. doi:<http://dx.doi.org/10.1016/j.compositesb.2008.12.002>.
- [8] Liu, B. (2001). *Two-Level Optimization of Composite Wing Structure Based on Panel Genetic Optimization*. Ph.D. thesis, Univeristy of Flodida.
- [9] Macquart, T., Bordogna, M. T., Lancelot, P., et al. (2016). Derivation and application of blending constraints in lamination parameter space for composite optimisation. *Composite Structures*, 135, 224 – 235. ISSN 0263-8223. doi:<http://dx.doi.org/10.1016/j.compstruct.2015.09.016>.
- [10] Bordogna, M. T., Macquart, T., Bettebghor, D., et al. (2016). Aeroelastic optimization of variable stiffness composite wing with blending constraints. 17th AIAA/ISSMO Multidisciplinary Analysis and Optimization Conference. doi:10.2514/6.2016-4122.
- [11] Adams, D. B., Watson, L. T., Gurdal, Z., et al. (2004). Genetic algorithm optimization and blending of composite laminates by locally reducing laminate thickness. *Advances in Engineering Software*, 35(1):35-43.
- [12] Campen, J. V., Seresta, O., Abdalla, M. M., et al. (2008). General blending definitions for stacking sequence design of composite laminate structure. 49th AIAA/ASME/ASCE/AHS/ASC structures, structural dynamics, and materials, pp. 7–10.
- [13] Tsai, S. W. and Hahn, H. T. (1980). *Introduction to composite materials*. Technomic Publishing Co.
- [14] Grenestedt, J. and Gudmundson, P. (1993). Layup optimization of composite material structures. In P. PEDERSEN (Ed.), *Optimal Design with Advanced Materials*. Oxford: Elsevier. ISBN 978-0-444-89869-2, pp. 311 – 336. doi:<http://dx.doi.org/10.1016/B978-0-444-89869-2.50027-5>.
- [15] Kang, B. S., Park, G. J., and Arora, J. S. (2006). A review of optimization of structures subjected to transient loads. *Structural and Multidisciplinary Optimization*, 31(2), 81–95.
- [16] Kang, B. S., Choi, W. S., and Park, G. J. (2001). Structural optimization under equivalent static loads transformed from dynamic loads based on displacement. *Structural and Multidisciplinary Optimization*, 79(2), 145–154.
- [17] Bettebghor, D., Blondeau, C., Toal, D., et al. (2013). Bi-objective optimization of pylon-engine-nacelle assembly. *Structural and Multidisciplinary Optimization*, 48(3), 637–652.
- [18] Park, G. J. (2006). Technical overview of the equivalent static loads method for non-linear static response structural optimization. *Structural and Multidisciplinary Optimization*, 43, 319–337.
- [19] (2016). *Optibless - an open-source toolbox for the optimisation of blended stacking sequences (accepted)*. In *The seventeenth European Conference on Composite Materials (ECCM17)*.

- [20] Raju, G., Wu, Z., and Weaver, P. (2014). On further developments of feasible region of lamination parameters for symmetric composite laminates. In *55th AIAA/ASME/ASCE/AHS/ASC Structures, Structural Dynamics, and Materials Conference, AIAA SciTech, (AIAA 2014-1374)*. doi:<http://dx.doi.org/10.2514/6.2014-1374>.
- [21] Ijsselmuiden, S. T., Abdalla, M. M., and Gurdal, Z. (2008). Implementation of strength-based failure criteria in the lamination parameter design space. *AIAA Journal*, 46(7), 1826–1834.
- [22] Vincenzo, F. G. D. (2012). Hybrid static aeroelasticity new capabilities - cfd data management.

## Acknowledgement

Paul Lancelot is grateful for the founding by the European Community's CleanSky 2 Programme under Horizon 2020 (H2020) under the Grant Agreement 686804. The ReLOAD project (Regional turboprop Loads control through active and passive technologies) is a CfP project funded under the Regional IADP involving 2 partners. The project started on 1 December 2015.

## Copyright statement

The authors confirm that they, and/or their company or organization, hold copyright on all of the original material included in this paper. The authors also confirm that they have obtained permission, from the copyright holder of any third party material included in this paper, to publish it as part of their paper. The authors confirm that they give permission, or have obtained permission from the copyright holder of this paper, for the publication and distribution of this paper as part of the IFASD-2017 proceedings or as individual off-prints from the proceedings.